Geometric Approaches for Modeling Movement Quality:

Applications in Motor Control and Therapy

by

Anirudh Som

A Thesis Presented in Partial Fulfillment
of the Requirements for the Degree
Master of Science

Approved April 2016 by the
Graduate Supervisory Committee:

Pavan Turaga, Chair
Narayanan Krishnamurthi
Andreas Spanias

ARIZONA STATE UNIVERSITY

May 2016

ABSTRACT

There has been tremendous technological advancement in the past two decades. Faster computers and improved sensing devices have broadened the research scope in computer vision. With these developments, the task of assessing the quality of human actions, is considered an important problem that needs to be tackled. Movement quality assessment finds wide range of application in motor control, health-care, rehabilitation and physical therapy. Home-based interactive physical therapy requires the ability to monitor, inform and assess the quality of everyday movements. Obtaining labeled data from trained therapists/experts is the main limitation, since it is both expensive and time consuming.

Motivated by recent studies in motor control and therapy, in this thesis an existing computational framework is used to assess balance impairment and disease severity in people suffering from Parkinson's disease. The framework uses high-dimensional shape descriptors of the reconstructed phase space, of the subjects' center of pressure (CoP) tracings while performing dynamical postural shifts. The performance of the framework is evaluated using a dataset collected from 43 healthy and 17 Parkinson's disease impaired subjects, and outperforms other methods, such as dynamical shift indices and use of chaotic invariants, in assessment of balance impairment.

In this thesis, an unsupervised method is also proposed that measures movement quality assessment of simple actions like sit-to-stand and dynamic posture shifts by modeling the deviation of a given movement from an ideal movement path in the configuration space, i.e. the quality of movement is directly related to similarity to the ideal trajectory, between the start and end pose. The $\mathcal{S}^1 \times \mathcal{S}^1$ configuration space was used to model the interaction of two joint angles in sit-to-stand actions, and the

$\mathbb{R}^2$ space was used to model the subject's CoP while performing dynamic posture shifts for application in movement quality estimation.

DEDICATION

I dedicate this thesis to my parents and grandparents, for without their love, support and encouragement, this would not have been possible.

ACKNOWLEDGMENTS

There are several people who have contributed towards this thesis. First, I would like to thank my thesis advisor Dr. Pavan Turaga, for showing confidence in me and for giving me the opportunity to work in his lab. His knowledge, guidance and constant support have kept me focused during the duration of my thesis.

I would also like to thank the other members of my thesis committee, Dr. Narayanan Krishnamurthi and Dr. Andreas Spanias, for their invaluable inputs and for taking time off their schedule to serve on my committee. I am also grateful to Dr. Vinay Venkataraman, Dr. Rushil Anirudh and Qiao Wang at ASU for introducing me to their area of research and helping me finish my thesis.

I am thankful to my graduate advisor, Sno Kleespies from the department of Electrical Computer and Energy Engineering at ASU, for helping me make my stay at ASU, a comfortable one.

This thesis would not have been possible without the love, guidance and unconditional support of my parents – Udayan Som and Maithreyi Som.

TABLE OF CONTENTS

CHAPTER Page

LIST OF TABLES

LIST OF FIGURES

Chapter 1

INTRODUCTION

1.1 Balance Impairment in Parkinson's Disease

Parkinson's disease (PD) is a chronic, progressive and idiopathic disorder of the central nervous system, mainly affecting motor control. In the United States, about one million people are affected by PD [1], and live with no cure. Some of the symptoms include – degradation of motor functions, speech, behavior and thought process. These symptoms continue and aggravate over time. It is considered to be the second most common age related neurodegenerative disease, and with aging population worldwide, the incidence of idiopathic PD will only increase [2]. The increasing demand for health-care and rehabilitation for the elderly, calls for efficient management guidelines offering effective assessment of impairment. The various motor symptoms that are shown by people suffering from PD include: tremor, bradykinesia (slowness of movement), rigidity and postural instability. Postural instability is the most common symptom affecting many activities of daily living and is shown to be the leading cause of falls in people with PD [3, 4, 5, 6].

Most widely, the research studies that investigated the impact of PD on health-related quality of life [7, 8] and balance involved using clinical scores and balance tests that are mainly based on visual evaluation of specified movement tasks by a trained medical personnel. At the most, they included calculation of walking speed, maximum time period for which one can stand quietly without taking a step on various surfaces, how far one can lean without losing balance or take a step. For example, the Unified

Parkinson's Disease Rating Scale (UPDRS) [9] involves subjective clinical observation, has been widely used by clinicians to follow the progression of the disease, especially the severity of the motor impairments, with 0 being least severe and 180 being most severe. Although this clinical scale has been widely used, the number of test items used to evaluate balance control is very less compared to the number of items used to assess various other impairments of the disease. In addition, evaluation based on visual examination may not be sufficient to identify subtle changes in balance. Only a minority of the studies utilized obtained sway measures (using CoP data) during quiet standing and balance perturbations. Given this, developing automated methods to quantitatively assess the level of impairment will be beneficial, and is the motivation for our research to develop a framework for automatic assessment of "quality" of posture shift movement. In this thesis, a standardized model to effectively assess the level of balance impairment across the subjects in the study is proposed. Towards this, analysis of the postural dynamic shifts dataset from healthy individuals and people with PD while standing on a force platform was done.

1.1.1 Related Work

Clinical assessment tools will be useful in assessing fall risk and to determine different types of balance deficits in subjects with PD. In [10], the authors studied the relevance of clinical balance assessment tools to differentiate balance deficits, indicating that the use of wearable sensors and objective measures of balance will lead to sensitive, specific and responsive clinical balance assessment. Schoneburg *et al.*[11], described a framework to characterize balance dysfunction using four postural control systems: balance during quiet stance; reactive postural adjustments; anticipatory postural adjustments and dynamic balance control.

Giuberti *et al.*[12], investigated whether kinematic variables like angular amplitude, speed of thighs' motion, obtained from a leg agility task, were representative of the UPDRS scores of subjects with PD. Lee *et al.*[13], used gait characteristics and wavelet-based features to classify idiopathic PD patients and healthy subjects, and achieved a classification accuracy of 77.33%. Khorasani *et al.*[14], used Hidden Markov Model with Gaussian mixtures to classify gait data collected from 16 healthy and 15 PD subjects, with an accuracy rate of 90.3%. Leddy *et al.*[15], in their study compared Functional Gait Assessment (FGA) and Balance Evaluation Systems Test (BESTest) over the Berg Balance Scale (BBS), and found both to be reliable and valid for assessing balance in PD subject, but with the BESTest approach being more sensitive for identifying fallers. [16, 17] used linear, Gaussian and polynomial kernel support vector machine (SVM) models to classify Minimum foot clearance (MFC) gait patterns into healthy elderly and balance impaired elderly classes. Greene *et al.*[18] also developed SVM models using standing balance trial information collected from elderly subjects to classify them into subjects with or without a history of falls.

Recent interest in the stroke rehabilitation community has been towards development of automated methods to quantitatively assess the quality of movement to aid in therapy treatment [19, 20, 21]. The main idea here is to extract feature representations from the wrist trajectory data collected from stroke survivors, and assess the level of impairment. In this thesis, we take this idea to assess the level of impairment in subjects with PD. The performance of various features is tested over the Dynamical Posture Shift data.

1.2 Movement Quality Assessment

In many applications for health-care, the ability to monitor, inform, and asses the quality of our movements, plays a key role. This ability can enable the creation of systems that one could use on an everyday basis while reducing the time and effort required on the part of trained physical therapist. Home based systems are also more intimate, and reduce the need to travel elsewhere for physical therapy. A growing class of affordable sensing devices have led to the development of such home-based and hospital-based systems that can provide feedback and quality ratings for movements. Sensors for motion capture (e.g. Optitrack, Microsoft Kinect), accelerometers and gyroscopes are often used in such systems. Similar ideas are also being studied in the context of sports and athletics [22].

In the effort to build autonomous systems, a large body of work combines features obtained from the sensor data with machine learning techniques to predict quality scores similar to a physical therapist/experts. This involves obtaining labeled data from therapists, which is used to train a model [23, 24, 22, 25]. Obtaining such labels is not easy, since domain knowledge is very essential in most applications for movement quality assessment. Additionally, physical therapists ratings may be subjective, with wide variability in rating across different therapists. One approach to decouple the inherent subjectivity of rating vs the true quality is via a combination of crowd sourcing platforms such as Amazon MTurk [26], with computational methods such as non-negative matrix factorization. This approach has been difficult to pursue in fields where experts are required to label data such as in physical therapy and medical imaging, and where sharing of patient data raises many concerns.

The role of geometric constraints in human body, and associated metrics for

measuring movement quality were considered. The proposed approach is based on recent studies which suggest that the most efficient movement between two poses, in certain well defined cases, is often the geodesic path in the pose-space [27]. Some of these results have been reported in other forms, such as showing that the optimal reaching movements in the Euclidean space appear curved [28, 29]. Recent work in motor control suggests that, when presented with visual feedback of the configuration space of two joints (more specifically, a torus), as applied to a reaching movement, subjects' movements tend to converge to geodesics on the torus [30].

These results suggest that the geometry of the configuration space may have an important role to play in creating effective, scalable algorithms for a variety of applications in interactive rehabilitation and physical therapy. While the basic scientific results reviewed above suggest a clear unifying framework in terms of optimal paths and geodesics, there are several engineering research problems that arise in practical implementation. Firstly, in order to create a general algorithmic framework, one needs to have a modular approach to plug in different kinds of configuration spaces as available from different sensing modalities: such as product-space of circles for joint angles obtained from motion-capture devices, or shape silhouettes from video sensors. Secondly, a study of the correlation between geometrically derived measures of quality, with other clinical measures of quality such as those obtained from force plates etc. is needed to throw light on the possibility of using them as surrogates of clinical measures. In this thesis, promising results are shown for quality analysis of human movement in the following case – a) movement quality of sit-to-stand actions performed by 4 healthy subjects; b) quality of dynamic postural shifts performed by 43 healthy and 17 Parkinson's disease impaired subjects. For the sit-to-stand actions, we consider the important feature to be the body-joint angles, measured between the

shoulder, hip and knee joints on the left and right side of the body. A pair of such angles is represented on the product space of two circles, $\mathcal{S}^1 \times \mathcal{S}^1$, a torus. For the dynamic postural shifts, the important feature is the centre of pressure (CoP) position in the mediolateral and the anteroposterior directions.

1.2.1 Related Work

Assessing the quality of everyday actions has tremendous scope in applications like sports, healthcare rehabilitation systems, exercise systems and so on. There have been several efforts to evaluate the performance of specific actions by using trajectory-based evaluation metrics [31, 32, 33]. Recent work has investigated the use of spatio-temporal pose features from video segments, for estimating quality of sports actions, such as diving and figure-skating [22]. This is based on learning a regression function from pose-features to quality scores, which does not give much insight into what constitutes good movement quality. Another line of work, in the field of stroke rehab therapy, the computational score is made more intuitive by breaking into interpretable components for assessment of reach movements of stroke survivors [20]. However, this analysis requires pre-specification of components from domain knowledge, and may not generalize to other domains.

Dynamical system theory and geometric techniques have also been employed for analysis of movement quality. Shape distribution functions of the reconstructed phase space have been used for classifying movements of unimpaired/healthy and stroke-impaired subjects [24]. This approach also requires training sets for regressing shape distributions to movement quality. Recently, Tao *et al.* [25] developed a method for online movement quality assessment of gait movement via hidden Markov modeling

of normal movements using Kinect skeleton data. Both these approaches required machine learning methodologies, and generally lack interpretability.

Recent work in biomechanics suggests that what constitutes good movement quality may have something to do with *geodesicness* of the movement in the configuration space. The idea that movements need not necessarily lie on straight line trajectories, but instead evolve along curved paths was suggested by Biess *et al.* [27]. These ideas were also demonstrated for finger tapping, while representing hand pose as a point on a product space of angles – in other words a torus [30].

1.3 Contributions

The contributions made in this thesis are listed below, that will be discussed in detail in further sections:

(a) Proposed a computational framework that utilizes attractor-shape descriptors of the reconstructed phase space from postural shits performed by subjects to –

- Perform three class classification of subjects into one of the following classes – healthy young, healthy old and subjects suffering from Parkinson's disease;
- Assess the level of disease severity and balance impairment in subjects having Parkinson's disease.

(b) Proposed to model the deviation of a given trajectory w.r.t. an ideal path as a measure of quality, on the $\mathcal{S}^1 \times \mathcal{S}^1$ pose-space for sit-to-stand actions and on the $\mathbb{R}^2$ space for the dynamic posture shifts movement.

- The proposed movement quality measure is evaluated by studying the correlation between the proposed method and other clinical movement quality measures.

1.4 Organization

Chapter 2 talks about dynamic modeling in computer vision, traditional dynamical invariant measures, shape distribution functions and describes the dataset, features and experimental results of the framework proposed for balance impairment assessment in subjects suffering from Parkinson's disease.

Chapter 3 describes the mathematical preliminaries of our other proposed movement quality measure for the sit-to-stand actions and the dynamic posture shift actions. It also gives details of the dataset used, experiments carried out and the visualization of the movement on the $\mathcal{S}^1 \times \mathcal{S}^1$ representation space.

Finally, chapter 4 presents conclusions and scope for future work.

Chapter 2

ASSESSMENT OF BALANCE IMPAIRMENT IN PARKINSON'S DISEASE

2.1 Dynamic Modeling in Computer Vision

Methods to model the dynamical properties of signals from various sensing platforms have been the foundation for various applications in computer vision, like human activity recognition and analysis [34], dynamical scene recognition [35] and so on. Human movements like walking, running, consist of periodic action sequences that repeat themselves with some variability [36]. Such properties of human movement that are descriptive of a complex nonlinear chaotic system have driven researchers to use the theory of nonlinear dynamical systems to model human movement [36, 37, 38, 39, 40, 41, 42, 43]. Capturing the changes of actions in both the spatial and temporal domain, can be achieved by defining a state space, and by learning a function that can map the current state space to the next one [44, 45]. Recent attempts have been made to obtain a direct representation of the dynamical system from the observed data by using tools from chaos theory. [37] try to estimate the dynamical system parameters like number of independent variables, degrees of freedom and other parameters, directly from the data. Traditional methods approximate the true-dynamics of the system by attempting to fit a model to the observed data. The method in [37] can help generalize representation without any strong assumptions, and is suitable for analyzing a wide range of dynamical phenomenon.

2.1.1 Analysis of Dynamical Systems

Dynamical systems are governed by a set of functions that define the variation in the behavior of the system over time. If these functions are linear or nonlinear, then the dynamical systems are linear or nonlinear respectively. State variables can be used to represent the state of a dynamical system at a given time t. A dynamical system is termed deterministic if there exists a unique future state for a given current state and is termed stochastic if the future state is derived from a probability distribution of possible states.

A chaotic system is a dynamical system with deterministic behavior that shows high sensitivity to initial conditions. The states in a chaotic system are comparable to an n-dimensional manifold, also known as the phase space. The chaotic system evolves over time in its phase space based on the system variables that govern the dynamics of the system. A trajectory is defined as the path traversed by the system over time and the phase space where the trajectories settle down as time approaches infinity is denoted as an attractor. An ideal scenario would be to have access to all independent variables of the system and their relationships in order to have a complete understanding of the system. However, in a real-world case, the data recorded if of low-dimension and in most cases is insufficient to model the underlying dynamics of the system. In addition, model-based parametric approaches like the Linear Dynamical System (LDS) assume an underlying mapping function f to describe the system's dynamics. For complex systems like that of human movement, it has been established that such approaches may not be suitable due to simplification of assumptions [46]. Chaotic systems help determine certain invariants of the function f without making any assumptions about the system.

2.1.2 Phase Space Reconstruction

All the possible states of a system can be represented on the phase space [47, 48]. For a deterministic dynamical system that can be mathematically modeled, the future states of the system can be determined using information of the present and past states. However, it gets more complex in the case of understanding human actions and dynamic scenes. In addition, sensing systems do not allow us to observe all the variables of the system. To address these problems, methods that reconstruct the attractor to obtain a phase space which preserves the important topological properties of the original dynamical system are required. We must find a function that can map between the 1-dimensional time series data and the m-dimensional attractor, with the assumption that all the variables of the system influence one another. The phase space reconstruction concept was explained in the embedding theorem proposed by Takens, called Takens' embedding theorem [49]. For a discrete dynamical system with a multidimensional phase space, the time-delay or embedding vectors are obtained by concatenating the time-delayed samples given by the following equation

$$\mathbf{x}_i(n) = [x_i(n), x_i(n+\tau), ..., x_i(n+(m-1)\tau)]^T \tag{2.1}$$

Here m is the embedding dimension and τ is the embedding delay. Careful selection of these parameters can help facilitate a good phase space reconstruction. If m is sufficiently large, then the important topological properties of the unknown multidimensional system can be reproduced in the reconstructed phase space [47]. The embedding method provides a way to apply theoretical concepts of nonlinear dynamical systems onto the observed time series data generated from low-dimensional deterministic dynamical systems. However, it does not provide us with a method to

estimate the optimal values of m and τ. The false nearest neighbors [50] approach can be used to estimate m and the first zero-crossing of the autocorrelation function [51] can be used to estimate τ.

2.1.3 Embedding Dimension

The embedding dimension m refers to the number of time-delayed samples concatenated to form the time-delay vector. The value of the integer embedding dimension must be estimated such that it can unfold the attractor thereby removing any self-overlaps due to projection of the attractor onto a lower dimensional space. Thus, the embedding dimension can also be defined as the minimum dimension required to completely unfold the attractor. Let us consider a vector in the reconstructed phase space in dimension m at time instant k, is given by

$$\mathbf{x}(k) = [x(k), x(k+\tau), ..., x(k+(m-1)\tau)]^T \tag{2.2}$$

The nearest neighbor in the reconstructed phase space is given by

$$\mathbf{x}^{NN}(k) = [x^{NN}(k), x^{NN}(k+\tau), ..., x^{NN}(k+(m-1)\tau)]^T \tag{2.3}$$

If the vector $\mathbf{x}^{NN}(k)$ is a false neighbor of $\mathbf{x}(k)$, then the embedding dimension m is unable to unfold the attractor. This can be avoided by moving to the next $m+1$ dimension, and this may move the false neighbor out of the neighborhood of $\mathbf{x}(k)$. The processing of finding false neighbors for every vector $\mathbf{x}_i(k)$, not only removes self-overlaps but also helps identify m where the attractor is completely unfolded. For human action trajectories the embedding dimension was found to be around 3 or 4 using the false nearest neighbor algorithm.

2.1.4 Embedding Delay

The embedding delay τ is the integer time delay used to construct the time-delay vector. In theory, the embedding process allows any value of τ, if one has access to accurate infinite data. The practical approach is to try finding a value for τ that makes the components of the vector $[x(k), x(k+\tau), x(k+2\tau)]^T$ in the embedding sufficiently independent. A low τ value makes adjacent components to be correlated and hence they cannot be considered as independent variables. However, a high τ value makes the adjacent components uncorrelated and almost independent, and thus it cannot be considered as part of the system that supposedly generated them. The shape of the embedded time series critically depends on the choice of τ. A good selection of τ should ensure that the data are maximally spread in phase space resulting in smooth phase space reconstruction. For strongly periodic data, the first zero crossing of the auto-correlation function is a suitable method to estimate the choice of τ.

2.2 Traditional Dynamical Invariants

2.2.1 Largest Lyapunov Exponent

The largest Lyapunov exponent (LLE) measures the average rate of divergence or convergence of initially closely-spaced trajectories over time [47, 48]. A positive Lyapunov exponent indicates orbital divergence and hence chaos in the system. A negative Lyapunov exponent indicates orbital convergence and hence a dissipative system. Chaos theory finds its applications in the analysis of chaotic dynamical systems. The LLE is a widely used measure of chaos in various fields like computer vision and biomechanics to model human actions, to quantify chaos in the reconstructed phase space and so on [36, 52, 35, 43, 38, 37]. Human movement is believed to exhibit a chaotic structure. The basic assumption here is that different action classes exhibit different levels of chaos, and quantification using LLE can help in the classification of these action classes.

2.2.1.1 Estimation of LLE (λ_1)

Rosentein [53] proposed a method to practically estimate LLE from time series data that quantifies chaos by monitoring the rate of divergence or convergence of closely spaced trajectories over time. The proposed algorithm is claimed to be easy, fast and robust to changes in embedding dimension, dataset size, embedding delay and noise. Rosentein's algorithm was developed to address the limitations of the Wolf's algorithm [54]. The flowchart for the Rosentein's algorithm can be seen in Figure 1. The largest Lyapunov exponent is given by

$$d_j(i) = d_j(0)e^{\lambda_1(i\Delta t)} \tag{2.4}$$

Here $d_j(0)$ is the initial separation in the phase space and $d_j(i)$ is the separation after i time steps of Δt. λ_1 is the largest Lyapunov exponent principal axes. The minimum number of data samples suggested by both Rosentein and Wolf, for accurate estimation of LLE is 10^m, where m is the embedding dimension. Hence, LLE may not be a suitable method to model short-duration time series data.

2.2.2 Correlation Sum

The correlation sum [47] is a chaotic invariant measure that is used to quantify density of points in the reconstructed phase space. For a point in the reconstructed phase space, a circle of radius r is drawn around it, and the number of points that lie inside the circle is counted. This procedure is repeated for all the points in the reconstructed phase space and can be mathematically represented by the following equation

$$C(r) = \frac{2}{N(N-1)} \sum_{j=1}^{N} \sum_{i=j+1}^{N} \Theta(r - d(\mathbf{x}(i), \mathbf{x}(j))) \tag{2.5}$$

where:

$$\Theta(a) = \begin{cases} 1, \text{ if } a \geq 0 \\ 0, \text{ otherwise} \end{cases}$$

and

$$d(\mathbf{x}(i), \mathbf{x}(j)) = \sqrt{\sum_{k=0}^{m-1} (X_{i-k} - X_{j-k})^2}$$

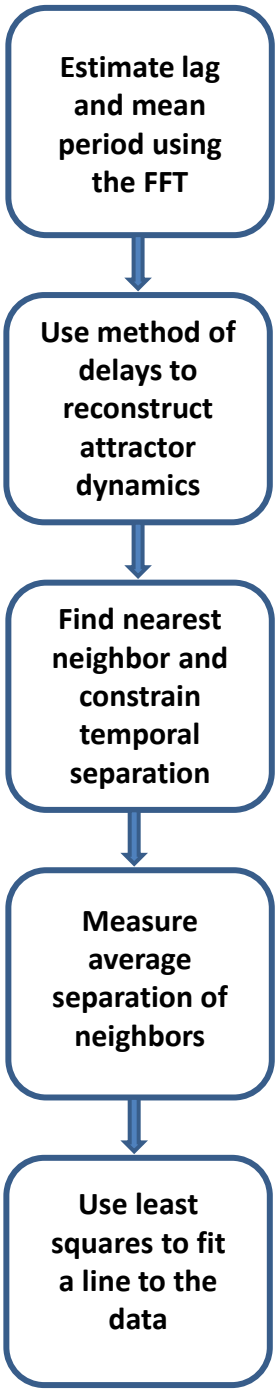

Figure 1. Rosentein's algorithm for estimation of LLE from experimental time series data.

Here Θ is the Heaviside function, $C(r)$ is called the correlation sum which converges to correlation integral when $N \to \infty$. This method of estimating the correlation sum is called the Grassberger-Procaccia algorithm. $C(r)$ refers to the probability that two randomly chosen vectors will be closer than r in the reconstructed phase space.

2.2.3 Correlation Dimension

One would expect the correlation sum $C(0) = 0$ for a chaotic system, as the points in the reconstructed phase space never repeat in a nonperiodic system embedded without false nearest neighbors. A plot of log $C(r)$ versus log r should given an approximately straight line whose slope in the limit of small r and large N is called as the correlation dimension [47] and is given by

$$D_2 = \lim_{r \to 0} \lim_{N \to \infty} \frac{\log C(r)}{\log r} \tag{2.6}$$

2.2.4 Drawbacks of Traditional Chaotic Invariants

The traditional chaotic invariant measures have been applied to model several visual dynamical phenomenon like video-based recognition of human actions [37], recognition of dynamical scenes [35]. However, these methods require large number of data samples of the order of $10^m - 30^m$ [52, 53] (m is the embedding dimension), for accurate estimation and with typical values of $m = 3$ and above, corresponding to a minimum of 1000 data samples.

The traditional chaotic invariants suffer from at least one of the following draw-

backs:(a) unreliable method in the case of small datasets, (b) computationally intensive, (c) relatively difficult to implement [53].

2.3 Shape Distribution Functions

In this section we will talk about the features that give information about the shape of the reconstructed phase space. The process of phase space reconstruction preserves certain topological properties. We consider the attractor as having its own characteristic shape in the high-dimensional phase space. The analysis of the shape of 3D surfaces is a well-studied problem in the computer vision community. Osada *et al.* [55] present a method for finding a similarity measure between 3D shapes. They do this by computing the shape distributions of the 3D surface sampled from the shape function by measuring their global geometric properties. For the experiments in this chapter, we will use the shape distribution of the reconstructed phase space as the dynamical feature representation. Some of the shape distribution functions [55] that are based on the geometric properties like distance, area are listed below:

(a) **D1**: measures the distance between one fixed point and one random point sampled from the reconstructed phase space. The fixed point is selected as the centroid of the attractor.

(b) **D2**: measures the distance between two random points in the phase space represented as $||\mathbf{x}_i - \mathbf{x}_j||_2$. Here $\mathbf{x}_i$ and $\mathbf{x}_j$ are the random points or embedding vectors in the reconstructed phase space.

(c) **D3**: measures the square root of the area of the triangle formed by three random points on the attractor

A set of these distances for randomly chosen embedding vector pairs are computed. A histogram is constructed from this set of distances by counting the number of samples which fall into each of $B = 50$ fixed sized bins, in order to get the shape distribution of the attractor. Studies [56] have shown that the **D2** global geometric

shape function performs better than the traditional chaotic invariant measures (LLE, correlation dimension and correlation sum).

2.4 Dataset for Evaluation

2.4.1 Subject Characteristics

The dynamical posture shifts dataset utilized for this study was collected as a part of a different study by Krishnamurthi *et al.* [57]. Regarding the dataset obtained from subjects with PD, the data was collected during medication-off state (12 hours after the last dosage of antiparkinsonian medication) from 17 patients (9 female, 8 male) with a mean age of 63.7 ± 4.9 years; ranging from 53 - 72 years with mild to moderate PD according to UK brain bank criteria with Hoehn & Yahr (H&Y) score from 2.5 to 3.0 with a stable medication regimen. Subjects were excluded from the study if they developed any of the following symptoms: dementia as defined by DSM-IV criteria; significant hepatic, renal, cardiovascular, cardiopulmonary, endocrinological issues; significant dyskinesia or on/off fluctuation; freezing-of-gait (FoG) leading to falls; other medical condition which would affect subjects' safety or compliance with the study procedures. For healthy individuals, the data was collected from a total of 43 young and elderly subjects with no known neurological or orthopedic disorders. Subjects less than 35 years were assigned to the young category and subjects older than 50 were assigned to the elderly category. 21 of the subjects (12 female, 9 male) fell in the young category (19-32 years) and had a mean age of 23.0 ± 3.8 years. 22 subjects (12 female, 10 male) fell in the elderly category (50-75 years) with a mean age of 62.7 ± 8.5 years at the time of enrollment. Approvals from appropriate Institutional Review Boards were obtained for data collection.

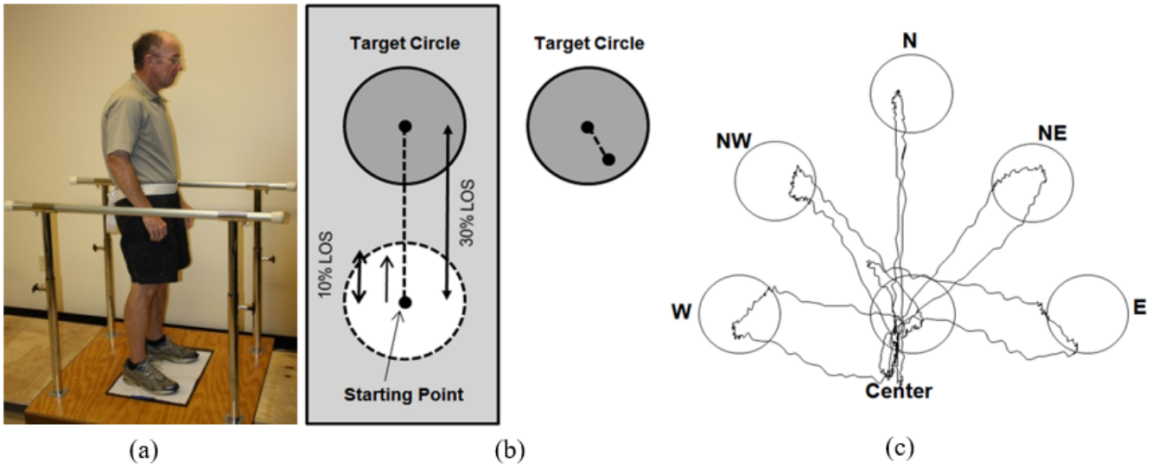

Figure 2. A subject with PD standing on the force platform during dynamic shifts looking at the monitor in front of him (not shown) at his eyes level; (b) The radius of the center and outward targets and distance between the center of starting circle and the target circle were chosen 10% and 30% of subjects' limits-of-stability (LoS) to facilitate comparison across subjects; (c) The targets along with typical CoP tracings during dynamic posture shifts of a trial were shown. The sequence of presentation of outward targets were randomized but the presentation of each outer target location was followed by presentation of the center target.

2.4.2 Dynamical Posture Shifts Data Collection

First, the subjects were instructed to stand on the force platform with their hands by their side and feet separated by hip-width. All subjects wore comfortable shoes. Once the subjects stood comfortably, the position of their feet on the force plate was traced to maintain consistent placement of the feet across trials. Previously developed LabVIEW-based graphical user interface was utilized to provide real-time visual feedback of the position of the subject's CoP [57]. At the start of the trial, the CoP of the subject was taken as the center of the center target. The subject viewed his/her CoP on the monitor placed in the front of the subject at eye level which provided real-time visual feedback. The goal for the subject is to move their CoP cursor from the center of the starting circle to the target circle and hold the

cursor as close as possible to the center of the target circle for 2 seconds. During the course of the trials, the outward targets were displayed in different positions, each separated by an angle of 45°.

The distance of the target circle from the center was set to 30% of the distance between the hip and the ankle, which has been demonstrated to be related to the LoS [58]. The radius of the center and target circles was set at 10% of the distance between the hip and the ankle. These facilitate comparison of performance across subjects. The subject was instructed to move their CoP, displayed in a form of red circular cursor, to the target circle position by leaning without lifting their feet off the ground. Once the subject maintained their CoP position as close as possible to the center of the target circle within the target for at least 2 seconds, the current target circle disappeared and the center target appeared which became the new target. If the subject was unable to stay within the target for at least 2 seconds, then the new target appeared automatically in 10 seconds. If the subject stayed inside the target for at least 2 seconds, the target was considered successfully achieved. The five different angles at which the targets presented were 0, 45, 90, 135, and 180 degrees. After reaching towards each target, the subject came back to the center target position before moving towards the next outward target. Thus, a total of ten targets were provided during the trial- O-0°, 0°-O, O-45°, 45°-O, O-90°, 90°-O, O-135°, 135°-O, O-180°, 180°-O, where O represents the origin or center target. During a single trial, 20 targets were presented, i.e. each of the ten targets were presented twice. The sequence of outward targets was randomly presented within and across trials to minimize learning effects or anticipation of the target. A total of five and three trials were performed by healthy subjects and subjects with PD, respectively, with sufficient rest periods in-between. For each trial, the following data were collected at 100 Hz:

CoP in mediolateral direction; CoP in anteroposterior direction; forces generated in x, y and z directions; and moments generated in x, y and z directions. Figure 2 shows an illustration of the real-time feedback paradigm used for data collection while performing dynamic posture shifts.

2.5 Features

2.5.1 Stabilogram Postural Indices

For each trial, a two-dimensional stabilogram was obtained from the CoP in the mediolateral and the anteroposterior directions. Many postural indices were calculated from three phases of each target presentation namely, (a) Initiation phase, (b) Movement Phase, and (c) Hold Phase. From the initiation and movement phases, corresponding time taken, path-length, and velocity were obtained [57]. From the hold phase, number of reentries, inaccuracy and unsteadiness (the mean and standard deviation, respectively, of the distances between the center of the target circle and the position of the CoP during the hold phase) were calculated. In addition, the peak velocity of CoP during the entire presentation was calculated.

The peak velocity is defined as the maximum velocity value that is calculated between two adjacent samples, from the time the CoP cursor leaves the starting point and completes the target reach. It is a sensitive measure that was found to distinguish postural control in people with PD for different deep brain stimulation (DBS) conditions. The peak velocity index can also help distinguish between healthy people and people suffering from PD. Bradykinesia and rigidity of movement is exhibited by people having PD. Healthy people do not exhibit Bradykinesia and therefore show higher peak velocity compared to people with PD.

2.5.2 Largest Lyapunov Exponent (LLE)

LLE is a widely used measure of chaos in various engineering applications, including biomechanics to model human movements for applications such as gait analysis [38]. It is a measure of average rate of divergence (or convergence) of initially closely-spaced trajectories over time [59]. The largest Lyapunov exponent is given by

$$d_j(i) = d_j(0)e^{\lambda_1(i\Delta t)} \tag{2.7}$$

where $d_j(0)$ is the initial separation in the phase space and $d_j(i)$ is the separation after i time steps of Δt. λ_1 is the largest Lyapunov exponent principal axes. Rosenstein's algorithm [53] was used to estimate LLE from real data in our experiments. The parameters of this feature include the embedding dimension (m) and the embedding delay (τ). In our experiments, the LLE features were extracted at $m = 3$ and $\tau = 5$.

2.5.3 D2 Shape Distribution

LLE requires a large number of data samples (of the order of 10^m – 30^m) for accurate estimation (where m is a parameter used in the estimation procedure called as the embedding dimension), with typical values of $m = 3$ and above, corresponding to a minimum of 1000 data samples. A recent approach proposed utilized ideas from shape analysis to achieve better classification and regression results in human activity analysis tasks [56, 60]. Using **D2** shape function from [55], the distance between two random vectors of the reconstructed phase space which is defined as

$$D_{ij} = ||\mathbf{x}_i - \mathbf{x}_j||_2 \tag{2.8}$$

where $\mathbf{x}_i$ and $\mathbf{x}_j$ are embedding vectors in the reconstructed phase space. A set of these distances for randomly chosen embedding vector pairs are computed. From this set, a histogram is constructed by counting the number of samples which fall into each of B = 50 fixed sized bins. The parameters that are required to be estimated include the embedding dimension (m) and the embedding delay (τ). The embedding dimension was fixed $m = 3$, and used the first zero-crossing of the auto-correlation function to estimate the value of τ [51].

2.6 Experiments and Results

2.6.1 3-class Classification

A total of 266 posture shift trials were collected, with each of the 17 PD subjects carried out 3 trials and each of the 43 healthy subjects (21 young and 22 elderly) carried out 5 trials. The extracted features in section IV were first passed through a k-Nearest Neighbor (K-NN) classifier. 3-class classification was done, with the three classes being PD, OLD and YNG. To assess the classifier's performance, 59 subjects were considered for the training set, 1 subject for the test set, and performed a round-robin leave-one-subject-out cross-validation. The advantage of using the K-NN classifier is that it does not have any hidden parameters that require tuning, thereby making it a very transparent technique for comparing different algorithms. The number of neighbors k was varied from $1, 2, ..., 51$. The classification accuracy of the K-NN classifier over the D2 shape distribution features is higher than LLE and peak velocity index features at all values of k, as seen in Figure 3. The best classification performance for D2 features was found at $k = 13$.

Next, the same experiment was performed using better classifiers like the linear-kernel Support Vector Machine (SVM) classifier. The parameter C was varied from $2^{-9}, 2^{-7}, ..., 2^{15}$. The classification accuracy over the D2 shape features is higher than LLE and peak velocity index features at almost all values of C, as seen in Figure 4. The linear-kernel SVM classifier was found to give best results at $C = 2^{-5}$. In Table 1, the classification accuracy of the K-NN classifier at $k = 13$, and the SVM classifier at $C = 2^{-3}$, after observing a recovery in the SVM's classification performance over the LLE features is shown. D2 shape distribution features gave the best classification

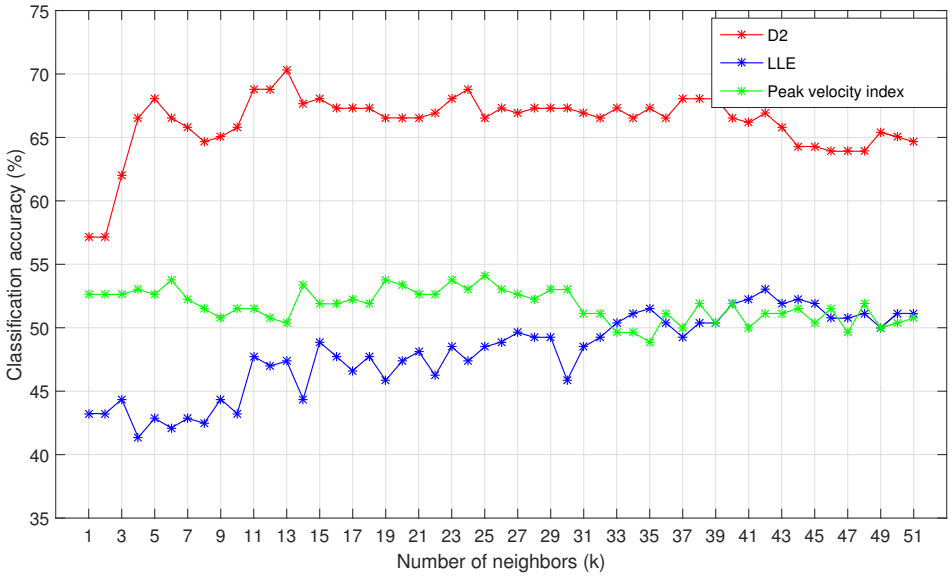

Figure 3. Classification accuracy of the K-NN classifier over the D2, LLE and peak velocity index features with k varying from $1, 2, ..., 51$.

result of 70.30% using the K-NN classifier at $k = 13$, and 73.68% using the SVM classifier at $C = 2^{-5}$. The confusion matrix for the 3-class classification of D2 features using the K-NN classifier can be seen in Table 2 and using the SVM classifier in Table 3.

Table 1. Classification accuracy of classifying PD, OLD and YNG classes, using K-NN classifier (k = 13) and linear-kernel SVM classifier (C = 0.125)

Feature	**K-NN (%)**	**SVM (%)**
Peak Velocity Index	50.38	53.01
LLE	47.37	47.37
D2	**70.30**	**71.43**

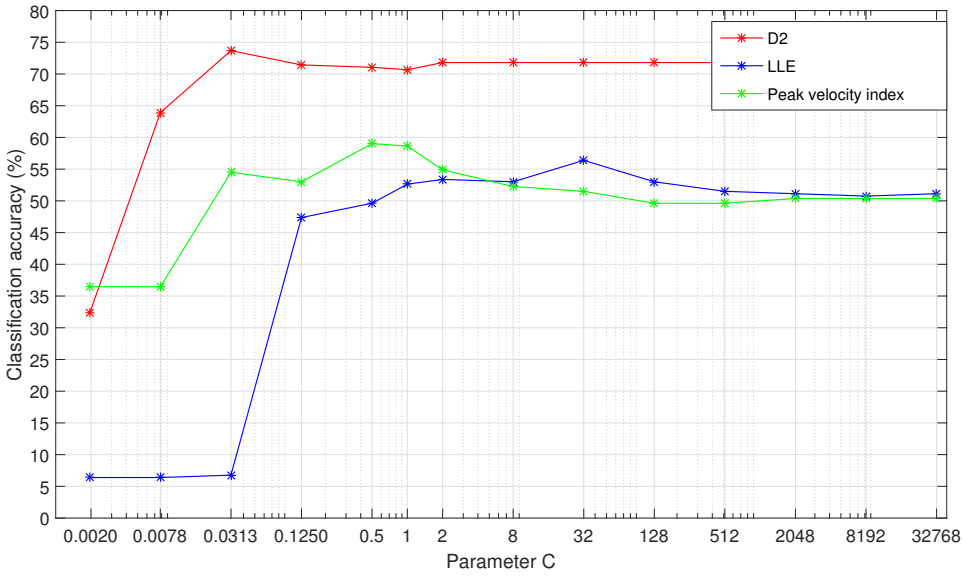

Figure 4. Classification accuracy of the linear-kernel SVM classifier over the D2, LLE and peak velocity index features with C varying from $2^{-9}, 2^{-7}, ..., 2^{15}$.

Table 2. The confusion matrix for the three-class classification problem using D2 shape distribution features over the K-NN classifier (k = 13)

	Predicted PD	**Predicted OLD**	**Predicted YNG**
Actual PD	**0.61**	0.33	0.06
Actual OLD	0.03	**0.78**	0.19
Actual YNG	0.01	0.32	**0.67**

Table 3. The confusion matrix for the three-class classification problem using D2 shape distribution features over the linear-kernel SVM classifier (C = 0.0313)

	Predicted PD	**Predicted OLD**	**Predicted YNG**
Actual PD	**0.80**	0.16	0.04
Actual OLD	0.06	**0.72**	0.22
Actual YNG	0.01	0.27	**0.72**

2.6.2 PD Severity Assessment

To assess the level of PD severity for the 17 PD subjects, a linear-kernel SVM regression model [61] was used. The total UPDRS score and the motor exam score

(part of the total UPDRS score) was used as an appropriate high level measure for the movement quality of the subjects, and also used to train two different regression models respectively. The total UPDRS score and motor exam score for all 43 healthy subjects was set to zero. Here too, a round-robin leave-one subject-out cross validation was carried out, by considered 59 subjects for the training set and 1 subject for the test set. The parameter C was varied from $2^{-9}, 2^{-7}, ..., 2^{15}$. The best regression model using the total UPDRS score and the motor exam score was obtained at $C = 10$ and $C = 4$ respectively. Negative predicted scores were forced to zero. Pearson correlation coefficient and p-values were calculated between the clinical and predicted scores, to quantify the performance of the regression model. The correlation coefficient and p-value pairs using the total UPDRS score and the motor exam score, for D2; LLE and peak velocity index features, can be seen in Table 4 and Table 5 respectively. Figure 5 displays the clinical and predicted total UPDRS scores, and Figure 6 displays the clinical and predicted motor exam scores for all 60 subjects.

Table 4. Pearson correlation coefficient and p-values between the predicted and clinical total UPDRS scores, using a Linear-kernel SVM regression model (C = 10)

Feature	**Correlation**	**P-value**
Peak Velocity Index	0.8135	$2.8227e^{-15}$
LLE	0.6449	$2.6707e^{-08}$
D2	**0.9006**	$\mathbf{1.1847}e^{-22}$

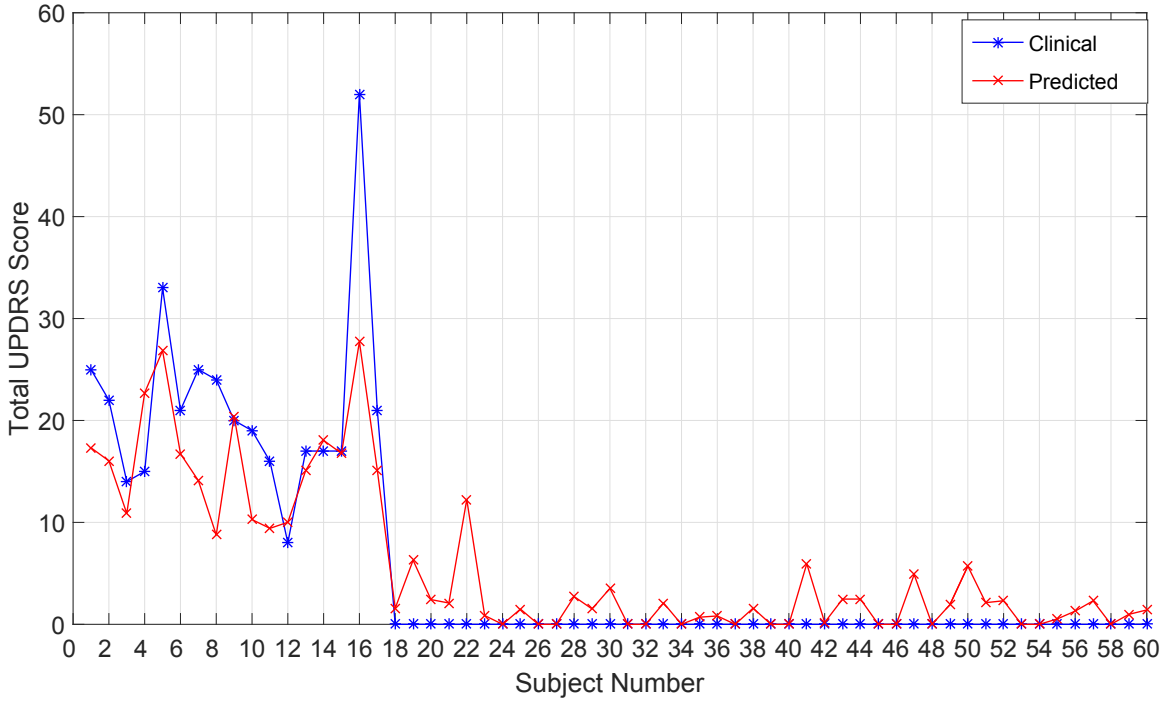

Figure 5. Comparison between clinical total UPDRS score and the predicted score, obtained using the D2 shape distribution feature, for 17 PD and 43 healthy subjects.

Table 5. Pearson correlation coefficient and p-values between the predicted and clinical motor exam scores, using a Linear-kernel SVM regression model (C = 4)

Feature	**Correlation**	**P-value**
Peak Velocity Index	0.6140	$1.8127e^{-07}$
LLE	0.6134	$1.8773e^{-07}$
D2	**0.8811**	$\mathbf{1.6320}e^{-20}$

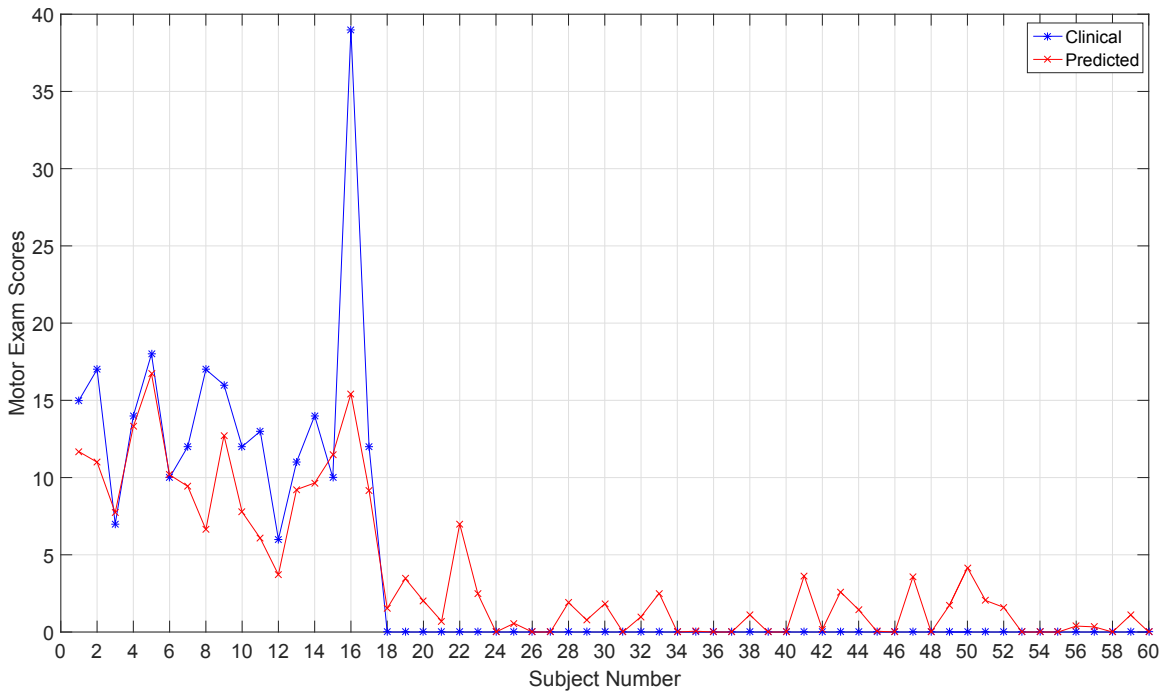

Figure 6. Comparison between clinical motor exam score and the predicted score, obtained using the D2 shape distribution feature, for 17 PD and 43 healthy subjects.

Chapter 3

MOVEMENT QUALITY ASSESSMENT OF SIT-TO-STAND ACTIONS

3.1 Mathematical Preliminaries

Here, we describe the geometric properties of the $\mathcal{S}^1 \times \mathcal{S}^1$ representation space.

3.1.1 Body-joint Angles on $\mathcal{S}^1 \times \mathcal{S}^1$

For this study, we considered the hip angles on the left and right side of the body as shown in Figure 7. The reason for using the left and right sides of the hip is to incorporate the symmetry of the action. It has been observed that symmetrical distribution of body weight under the feet, significantly improves STS actions in subjects suffering from hemiplegic stroke [62]. In other studies, improvements in postural stance was found to be correlated to postural symmetry as well [63].

Each of these angles can be represented equivalently on the circle, $\mathcal{S}^1$, and the angles computed from both the left and right side can be represented in the product space $\mathcal{S}^1 \times \mathcal{S}^1$ which is the torus T^2. This space possesses a Riemannian structure obtained by inheriting the Riemannian metric from $\mathbb{R}^2$ on the circle $\mathcal{S}^1 \subset \mathbb{R}^2$. Although the geodesics are inherited from the geodesic on $\mathcal{S}^1$, the actual metric on T^2 is a design choice. We will use a simple combination of the sum of the length of the shortest arc on the individual circles as our metric. This distance is defined as $d : \mathcal{S}^1 \times \mathcal{S}^1 \to \mathbb{R}$

$$d_{\mathcal{S}}(\theta_1, \theta_2) = \arccos(\cos(\theta_1 - \theta_2)), \tag{3.1}$$

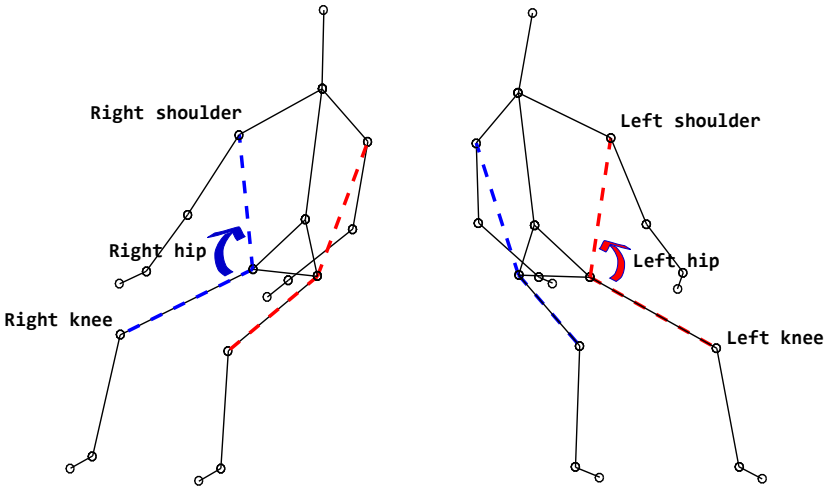

Figure 7. Illustration of the angles computed between different body joints in sit position.

Next, the distance on the torus between points $p_1 = (\phi_1, \theta_1)$ and $p_2 = (\phi_2, \theta_2)$ is given by $d_{\mathrm{T}}(p_1, p_2) = \sqrt{d_{\mathcal{S}}(\phi_1, \phi_2)^2 + d_{\mathcal{S}}(\theta_1, \theta_2)^2}$.

3.2 Measure of Quality

In this section, we outline the proposed approach that is used to quantify movement quality. We will refer to this approach as the summative measure. It requires observing the full trajectory of movement.

3.2.1 Summative Quality Measure

The idea of summative quality centers around measuring the deviation of a given trajectory compared to an idealized trajectory. Here, the idealized trajectory corresponds to the simple geodesic. To keep things simple, we will make it specific to the torus, where the idealized trajectory is fixed to the geodesic between the start and the end pose.

The geodesic on a circle is the shortest arc that connects two points, where the metric is defined as in (3.1). In order to compare a movement trajectory with the geodesic, we must first sample along the geodesic. Let $\gamma(t)$ represent the trajectory for which we wish to estimate a quality score. Further, let $\widetilde{\gamma}(t)$ represent the geodesic path with the same starting and ending points as $\gamma(t)$, i.e., $\gamma(0) = \widetilde{\gamma}(0)$ and $\gamma(1) = \widetilde{\gamma}(1)$. Let us then define the geodesic discretization interval to be given by $\delta = \frac{d_{\mathcal{S}}(\gamma(1),\gamma(0))}{N-1}$, where N is the number of desired samples along $\gamma(t)$. Since our operations are on the circle, $\mathcal{S}^1$, we are able to uniformly sample along the geodesic using δ as $\widetilde{\gamma}(t) = \gamma(0) + (t\ \delta)$. The sampled geodesic at 'time' t, is given by

$$\widetilde{\gamma}(t) = \begin{cases} \gamma(0) + (t\ \delta), & \text{if } (L > \pi) \text{ or } (-\pi < L < 0) \\ \gamma(0) - (t\ \delta), & \text{else.} \end{cases} \tag{3.2}$$

Here, $L = \gamma(0) - \gamma(1)$.

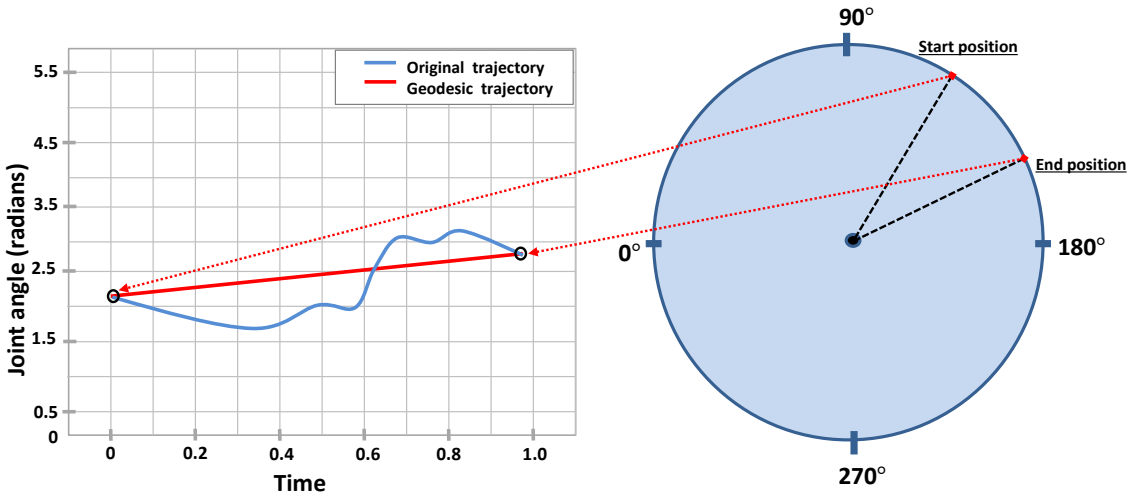

Figure 8. Comparison of the variation of the joint angle between the original trajectory and the geodesic trajectory, measured between the start and end positions of a given movement.

Once the angles for both the original and geodesic trajectory have been computed, we solve the registration problem between the two trajectories using Dynamic Time Warping (DTW) [64]. Figure 8 show the variation of the joint angle with time and how the geodesic trajectory can be visualized on the $\mathcal{S}^1$ representation space. The dissimilarity obtained using DTW is used as the final quality score, which is given by $q = \text{DTW}(\gamma_\phi(t), \widetilde{\gamma}_\phi(t)) + \text{DTW}(\gamma_\theta(t), \widetilde{\gamma}_\theta(t))$. Where $\gamma_\theta(t)$ and $\gamma_\phi(t)$ refer to the movement trajectories corresponding to first and second angles, θ and ϕ, respectively. For the sit-to-stand experiment, we use the above approach.

3.3 Dataset for Evaluation

3.3.1 Sit-to-stand Action Dataset

The data collected from the experimental protocol reported in [65], was obtained using a Microsoft Kinect sensor. The data consists of the 3D position information of the 20 body joints for four healthy subjects. Each of the subjects was first asked to perform a few sit-to-stand (STS) actions in their normal habitual manner. Next, each subject was asked to practice with the system for 10 minutes after being given few verbal instructions. The subjects were instructed to perform the STS actions in a relaxed, smooth manner, with their head guiding the whole body. They were also instructed to make sure that they moved forward and up at the same time. These STS actions come under the control (CT) stage. After resting for an hour, each subject was again asked to practice with the system for 10 minutes, but this time with auditory feedback and these STS action come under the feedback (FB) stage. On a whole, each subject carried out 12 STS actions during the CT stage and 21 STS actions during the FB stage. For subject 2, results are shown for only 9 STS actions in CT stage and 21 STS actions in FB stage, due to data recording problems. The findings reported in [65], indicate that the quality performance of all the four subjects generally improved with practice. The measure of quality was the velocity of the head trajectory. The improvement was also greater when auditory feedback was present. Since there are no ground truth scores in this dataset, we propose to generate quality scores for each movement, and show that our measures depict the same trend reported in [65] which is – movement quality becomes better with practice.

3.3.2 Dynamic Posture Shifts Dataset

The dataset contains time-series data of dynamic postural shifts of the subjects' Centre-of-Pressure tracings, collected from 21 healthy young subjects, 22 healthy elderly subjects and 17 subjects suffering from Parkinson's disease. Information on the subjects' characteristics and data collection procedure can be found in section 2.4.1 and section 2.4.2 respectively. We will use this dataset for the 2-class classification experiment discussed in section 3.4.2.

3.4 Experiments and Results

3.4.1 Sit-to-stand Movement Quality Assessment

We extract angle information from two sets of joints for each STS action. First we compute the angles between the left and right shoulder, hip and knee joints respectively as illustrated in 7. This ensures that the postural symmetry of the subject is considered while calculating the quality score. The final score is measured by computing the DTW distance between the movement trajectory and the corresponding geodesic path between the start and end poses, as described in section 3.2.1. A smaller DTW score is indicative of a well executed STS movement and a higher score indicates a poorer quality of movement.

The results of this experiment are shown in Figure 9,10,11,12. We show the quality scores across all STS movements carried out by each of the 4 subjects. To better indicate the trends for each subject, we also show the least squares fit line for the CT stage, FB stage and across all the STS sessions. We see no improvement for Subjects 2 and 3 during the CT stage as shown by the control group (CT) line fit. However, both subjects improve their movements during the FB stage as shown by the FB line fit. Subjects 1 and 4 show lower quality scores as the number of sessions in the CT stage progresses and continue to improve their movements during the FB stage as well. On the whole, all four subjects show a tendency to learn while performing the STS actions with each progressing session as clearly seen from the total line fit plot for each subject. These results follow the same trend reported in [65].

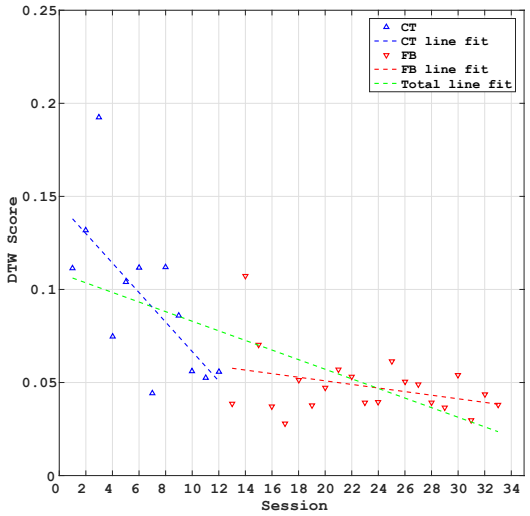

Figure 9. Comparison between DWT score and session number for Subject 1, to illustrate the change in quality of motion with practice. CT indicates the control stage, receiving no feedback. FB indicates the feedback stage, where feedback is given to enable better movement. The downward trend is clearly visible from the total line fit.

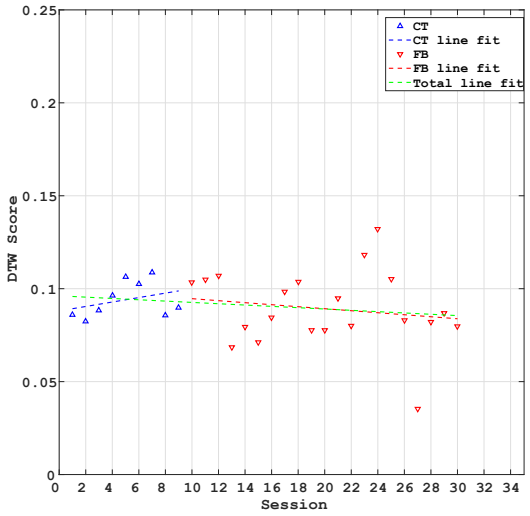

Figure 10. Comparison between DWT score and session number for Subject 2, to illustrate the change in quality of motion with practice. CT indicates the control stage, receiving no feedback. FB indicates the feedback stage, where feedback is given to enable better movement. The downward trend is clearly visible from the total line fit.

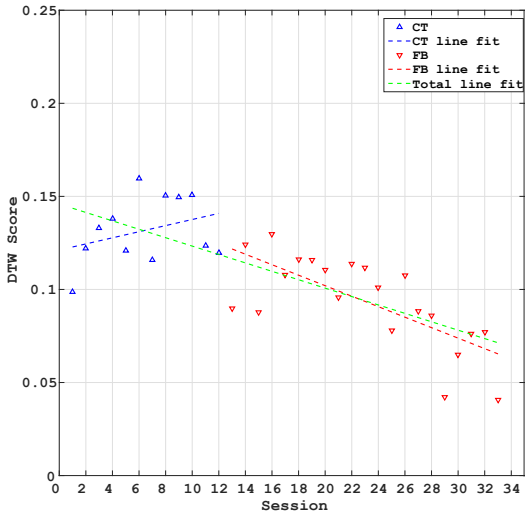

Figure 11. Comparison between DWT score and session number for Subject 3, to illustrate the change in quality of motion with practice. CT indicates the control stage, receiving no feedback. FB indicates the feedback stage, where feedback is given to enable better movement. The downward trend is clearly visible from the total line fit.

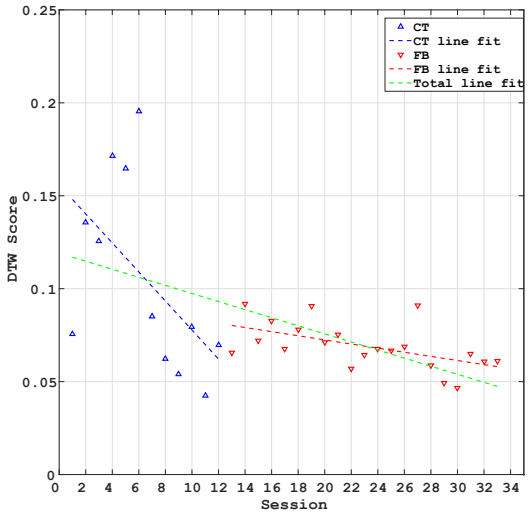

Figure 12. Comparison between DWT score and session number for Subject 4, to illustrate the change in quality of motion with practice. CT indicates the control stage, receiving no feedback. FB indicates the feedback stage, where feedback is given to enable better movement. The downward trend is clearly visible from the total line fit.

3.4.1.1 Visualization on the $\mathcal{S}^1 \times \mathcal{S}^1$ Representation Space

Figure 13 illustrates an example of the variation of the individual angles – θ and ϕ with time, for a STS session in the CT stage, with no feedback. θ and ϕ correspond to the joint angle between the left and right shoulder, hip and knee joints respectively. The proposed summative score for this session was equal to 0.22127, indicating a relatively low match with respect to the geodesic, i.e. a low quality movement. Figure 14 shows the variation on the $\mathcal{S}^1 \times \mathcal{S}^1$ representation space for the same example in the CT stage.

Similarly, Figure 15 shows an example of the variation of the individual angles θ and ϕ with time, for a STS session in the FB stage, where real-time auditory feedback was given. The proposed summative score for this session was equal to 0.048226, which is lower than the previous CT stage example and is also indicative of a close match to the ideal geodesic, i.e. a high quality movement. Figure 16 shows the variation on the $\mathcal{S}^1 \times \mathcal{S}^1$ representation space for the same example in the FB stage.

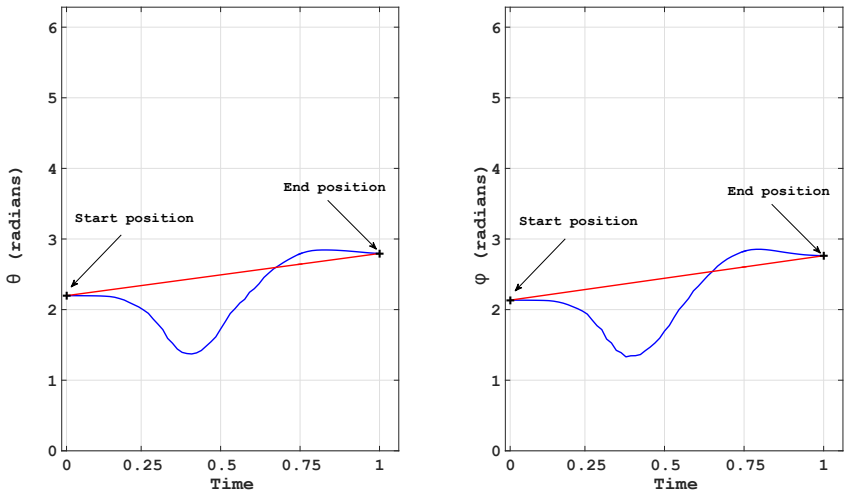

Figure 13. Variation of individual joint angles with time during CT stage. θ represents the joint angle between the left-shoulder, left-hip and left-knee; ϕ represents the joint angle between the right-shoulder, right-hip and right-knee. The trajectory shown with blue represents the original trajectory and the trajectory shown with red represents the geodesic.

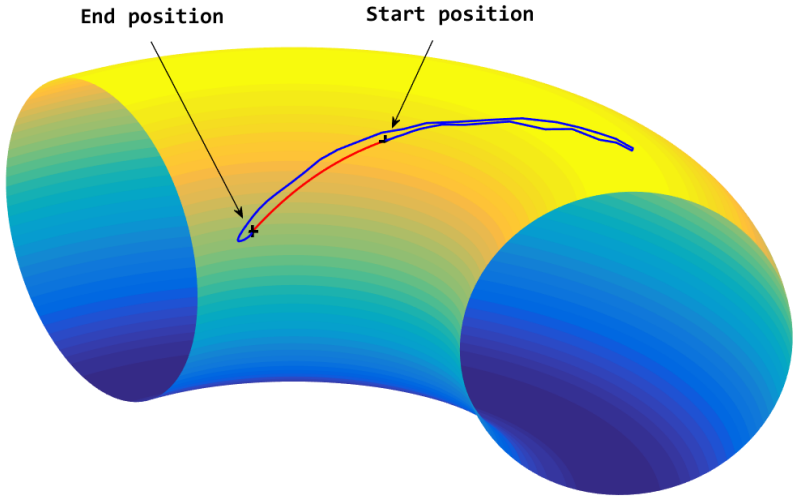

Figure 14. STS action on the $\mathcal{S}^1 \times \mathcal{S}^1$ configuration space during CT stage. θ represents the joint angle between the left-shoulder, left-hip and left-knee; ϕ represents the joint angle between the right-shoulder, right-hip and right-knee. The trajectory shown with blue represents the original trajectory and the trajectory shown with red represents the geodesic.

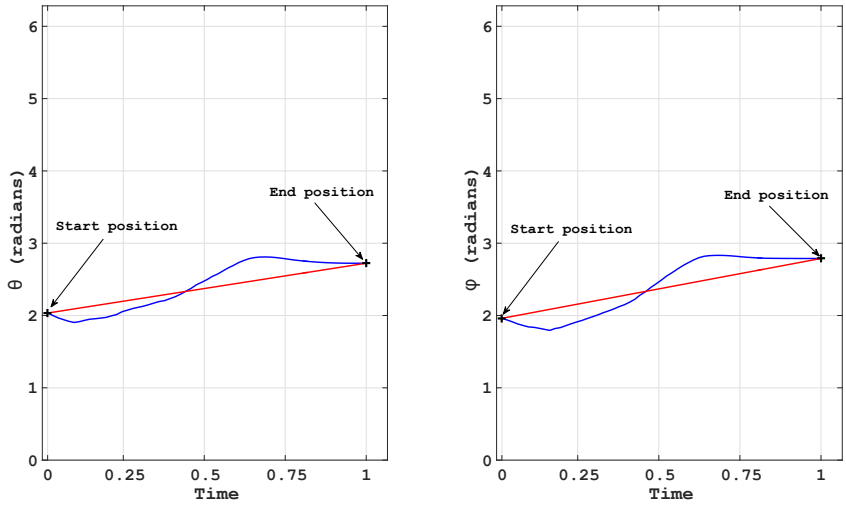

Figure 15. Variation of individual joint angles with time during FB stage. θ represents the joint angle between the left-shoulder, left-hip and left-knee; ϕ represents the joint angle between the right-shoulder, right-hip and right-knee. The trajectory shown with blue represents the original trajectory and the trajectory shown with red represents the geodesic.

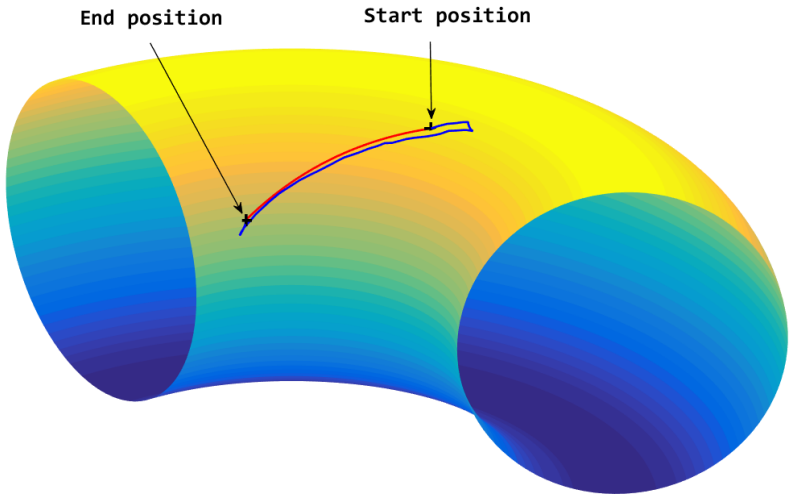

Figure 16. STS action on the $\mathcal{S}^1 \times \mathcal{S}^1$ configuration space during FB stage. θ represents the joint angle between the left-shoulder, left-hip and left-knee; ϕ represents the joint angle between the right-shoulder, right-hip and right-knee. The trajectory shown with blue represents the original trajectory and the trajectory shown with red represents the geodesic.

3.4.2 2-class Classification

Each of the 17 PD subjects performed 3 posture shift trials and each of the 43 healthy subjects (22 elderly and 21 young) performed 5 trials, thereby giving a total of 266 posture shift trials. Each trial consisted of 20 movements of the subject's CoP position from the start position to the target position.

The CoP's position in the mediolateral denoted by 'x'and the anteroposterior direction denoted by 'y', was used to calculate the DTW score. The straight path from the start position to the end position was considered to be the ideal movement path for each movement. The distance function used to calculate the distance between any two points $p_1 = (x_1, y_1)$ and $p_2 = (x_2, y_2)$ in the given trajectory is given by $d_{\mathrm{T}}(p_1, p_2) = \sqrt{(x_1 - x_2)^2 + (y_1 - y_2)^2}$. The final quality score obtained using DTW, is given by $q = \mathrm{DTW}(x(t), \widetilde{x}(t)) + \mathrm{DTW}(y(t), \widetilde{y}(t))$. Here, $x(t)$ and $y(t)$ refer to the given movement trajectories; $\widetilde{x}(t)$ and $\widetilde{y}(t)$ refer to the ideal movement trajectories. After computing the deviation of a given movement w.r.t. the ideal trajectory for all 20 movements, the computed deviations are summed up to give the DTW score for each trial. The final DTW score for each subject is obtained by averaging the DTW scores across all the trials.

The DTW scores for the 17 PD and 43 healthy subjects is shown in Figure 17. We would expect the final DTW score for PD subjects to be higher than healthy subjects. However, from the dynamic posture shifts data, the PD subjects performed their movements slowly and their total path length for each movement was smaller when compared to the healthy subjects. The slowness of the PD subjects' movement might have led to a more direct movement, thereby resulting in the observed reduction in their path length [57]. In agreement with the speed-accuracy trade-off effect,

bradykinesia of PD patients may ensure accuracy of movement [66], a hypothesis further supported by the study made by Krishnamurthi *et al.* [57], demonstrating that accurate CoP targeting (i.e. reduced path lengths) correspond to longer movement times in PD patients.

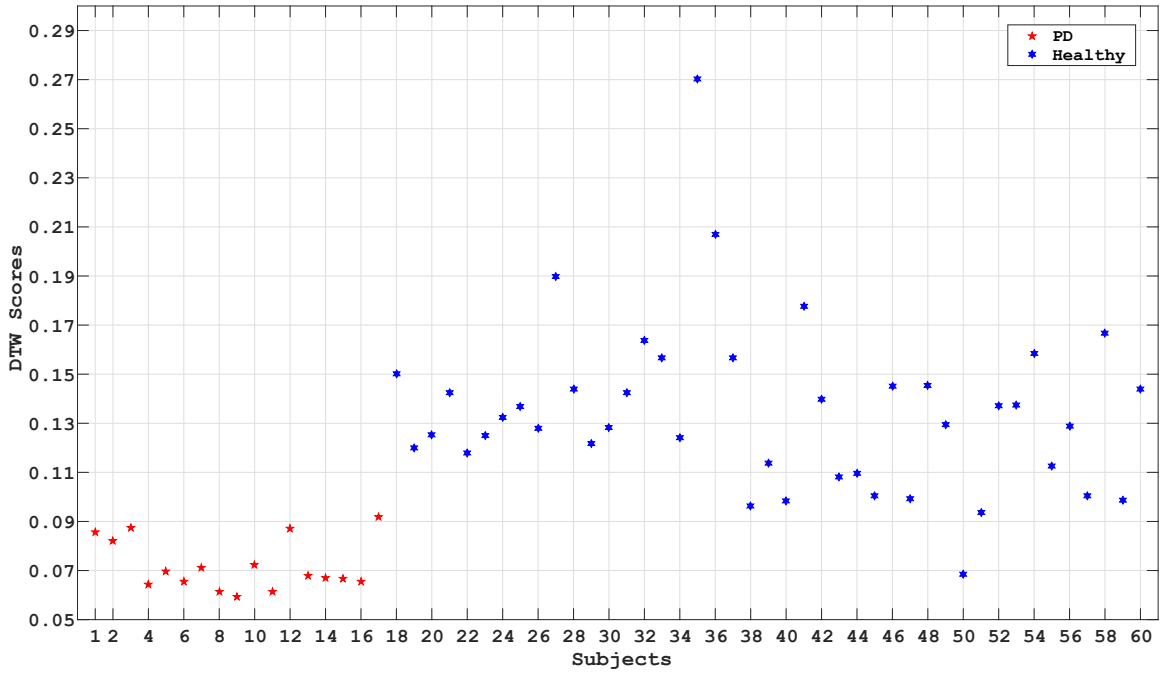

Figure 17. DTW score plot for 17 PD and 43 healthy subjects.

The D2 shape function was used as a baseline feature. To compute the D2 shape function, the following time-series information was used: the CoP in mediolateral direction; CoP in anteroposterior direction; forces in x, y and z directions; moments in x, y and z directions. The extracted features were passed through a 1-Nearest Neighbor (1-NN) classifier. 2-class classification was done, with the two classes being PD and Healthy. The classifier's performance was evaluated by considering 59 subjects for the training set and 1 subject for the test set, and performed a round-robin leave-one-subject out cross validation. Comparison of the classification performance

of the 1-NN classifier using the D2 shape features and DTW scores is shown in Table 6. The confusion matrix for the 2-class classification problem using the 1-NN classifier over the extracted D2 shape function features and computed DTW scores can be seen in Table 7 and Table 8 respectively. The DTW score only needed the subject's CoP position and was able to give a better classification performance, compared to the D2 shape feature that needed more information.

Table 6. Comparison of the classification accuracy of classifying PD and Healthy classes, using 1-NN classifier over the D2 shape and DTW score features

Feature	**1-NN (%)**
D2	87.97
DTW score	**91.67**

Table 7. The confusion matrix for the two-class classification problem using D2 shape distribution features over the 1-NN classifier

	Predicted PD	**Predicted Healthy**
True PD	**0.71**	0.29
True Healthy	0.05	**0.95**

Table 8. The confusion matrix for the two-class classification problem using DTW score as the feature over the 1-NN classifier

	Predicted PD	**Predicted Healthy**
True PD	**0.82**	0.18
True Healthy	0.05	**0.95**

Chapter 4

CONCLUSION AND FUTURE WORK

In this thesis, the use of attractor-shape descriptors to assess balance impairment from posture shifts in subjects having PD was proposed, as described in chapter 2. The effectiveness of the proposed descriptor was shown by the following experiments: 3-class classification of PD, old and young subjects and prediction of the total UPDRS scores and motor exam scores. The results are promising and show that the descriptor can significantly outperform other baseline features. In future, studies can be designed to investigate the potential of the proposed framework to assess disease severity of PD patients at their homes. The dynamic posture shifts data can be collected at the home setup using wearable sensors and these new datasets can also be incorporated to the existing datasets to improve the disease severity assessment.

In chapter 3, an unsupervised framework was proposed that uses the deviation from the ideal path of a trajectory in an appropriate pose-space, to measure movement quality. We apply the methodology to sit-to-stand movements, interpreted as a curve on the torus, $\mathcal{S}^1 \times \mathcal{S}^1$. We also applied the proposed framework to dynamic posture shifts data collected from healthy and Parkinson's disease impaired subjects. Our experimental results look promising and show the effectiveness of the proposed framework. This points the way toward more complex full-body quality assessments, that could utilize geodesicness measures on general shape manifolds. The DTW quality score can also be generalized to include true elastic invariant metrics such as those developed by Su *et al.* [67].

REFERENCES

[1] N. I. of Neurological Disorders and Stroke, "Parkinson's disease: Challenges, progress, and promise," tech. rep., National Institutes of Health, 2015.

[2] A. Reeve, E. Simcox, and D. Turnbull, "Ageing and parkinson's disease: why is advancing age the biggest risk factor?," *Ageing Research Reviews*, vol. 14, pp. 19–30, 2014.

[3] B. R. Bloem, J. P. Van Vugt, and D. J. Beckley, "Postural instability and falls in parkinson's disease.," *Advances in Neurology*, vol. 87, pp. 209–223, 2001.

[4] D. J. Beckley, V. P. Panzer, M. P. Remler, L. B. Ilog, and B. R. Bloem, "Clinical correlates of motor performance during paced postural tasks in parkinson's disease," *Journal of the Neurological Sciences*, vol. 132, no. 2, pp. 133–138, 1995.

[5] B. R. Bloem, D. J. Beckley, J. G. Van Dijk, A. H. Zwinderman, M. P. Remler, and R. A. Roos, "Influence of dopaminergic medication on automatic postural responses and balance impairment in parkinson's disease," *Movement Disorders*, vol. 11, no. 5, pp. 509–521, 1996.

[6] B. R. Bloem, D. J. Beckley, B. J. van Hilten, and R. A. Roos, "Clinimetrics of postural instability in parkinson's disease," *Journal of Neurology*, vol. 245, no. 10, pp. 669–673, 1998.

[7] G. P. D. S. S. Committee *et al.*, "Factors impacting on quality of life in parkinson's disease: results from an international survey.," *Movement disorders: official journal of the Movement Disorder Society*, vol. 17, no. 1, pp. 60–67, 2002.

[8] A. Schrag, M. Jahanshahi, and N. Quinn, "What contributes to quality of life in patients with parkinson's disease?," *Journal of Neurology, Neurosurgery & Psychiatry*, vol. 69, no. 3, pp. 308–312, 2000.

[9] C. Ramaker, J. Marinus, A. M. Stiggelbout, and B. J. van Hilten, "Systematic evaluation of rating scales for impairment and disability in parkinson's disease," *Movement Disorders*, vol. 17, no. 5, pp. 867–876, 2002.

[10] M. Mancini and F. B. Horak, "The relevance of clinical balance assessment tools to differentiate balance deficits," *European Journal of Physical and Rehabilitation Medicine*, vol. 46, no. 2, pp. 239–248, 2010.

[11] B. Schoneburg, M. Mancini, F. Horak, and J. G. Nutt, "Framework for understanding balance dysfunction in parkinson's disease," *Movement Disorders*, vol. 28, no. 11, pp. 1474–1482, 2013.

[12] M. Giuberti, G. Ferrari, L. Contin, V. Cimolin, C. Azzaro, G. Albani, and A. Mauro, "Assigning updrs scores in the leg agility task of parkinsonians: Can it be done through bsn-based kinematic variables?," *Internet of Things Journal, IEEE*, vol. 2, no. 1, pp. 41–51, 2015.

[13] S.-H. Lee and J. S. Lim, "Parkinson's disease classification using gait characteristics and wavelet-based feature extraction," *Expert Systems with Applications*, vol. 39, no. 8, pp. 7338–7344, 2012.

[14] A. Khorasani and M. R. Daliri, "Hmm for classification of parkinson's disease based on the raw gait data," *Journal of Medical Systems*, vol. 38, pp. 1–6, 2014.

[15] A. L. Leddy, B. E. Crowner, and G. M. Earhart, "Functional gait assessment and balance evaluation system test: reliability, validity, sensitivity, and specificity for identifying individuals with parkinson disease who fall," *Physical Therapy*, vol. 91, no. 1, pp. 102–113, 2011.

[16] R. Begg, D. Lai, S. Taylor, and M. Palaniswami, "Svm models in the diagnosis of balance impairments," in *3rd International Conference on Intelligent Sensing and Information Processing (ICISIP)*, pp. 248–253, IEEE, 2005.

[17] D. T. Lai, R. Begg, and M. Palaniswami, "Svm models for diagnosing balance problems using statistical features of the mtc signal," *International Journal of Computational Intelligence and Applications*, vol. 7, no. 03, pp. 317–331, 2008.

[18] B. R. Greene, D. McGrath, L. Walsh, E. P. Doheny, D. McKeown, C. Garattini, C. Cunningham, L. Crosby, B. Caulfield, and R. A. Kenny, "Quantitative falls risk estimation through multi-sensor assessment of standing balance," *Physiological measurement*, vol. 33, no. 12, pp. 2049–2063, 2012.

[19] Y. Chen, M. Duff, N. Lehrer, H. Sundaram, J. He, S. L. Wolf, T. Rikakis, T. D. Pham, X. Zhou, H. Tanaka, *et al.*, "A computational framework for quantitative evaluation of movement during rehabilitation," in *AIP Conference Proceedings-American Institute of Physics*, vol. 1371, pp. 317–326, 2011.

[20] V. Venkataraman, P. Turaga, M. Baran, N. Lehrer, L. Cheng, T. Rikakis, S. Wolf, *et al.*, "Component-level tuning of kinematic features from composite therapist impressions of movement quality.," *IEEE Journal of Biomedical and Health Informatics*, 2014.

[21] V. Venkataraman, P. Turaga, N. Lehrer, M. Baran, T. Rikakis, and S. L. Wolf, "Decision support for stroke rehabilitation therapy via describable attribute-based decision trees," in *International Conference of the IEEE Engineering in Medicine and Biology Society (EMBC)*, pp. 3154–3159, 2014.

[22] H. Pirsiavash, C. Vondrick, and A. Torralba, "Assessing the quality of actions," in *Computer Vision–ECCV 2014*, pp. 556–571, Springer, 2014.

[23] Y. Chen, M. Duff, N. Lehrer, H. Sundaram, J. He, S. L. Wolf, T. Rikakis, T. D. Pham, X. Zhou, H. Tanaka, *et al.*, "A computational framework for quantitative evaluation of movement during rehabilitation," in *AIP Conference Proceedings-American Institute of Physics*, vol. 1371, p. 317, 2011.

[24] V. Venkataraman and P. Turaga, "Shape descriptions of nonlinear dynamical systems for video-based inference," *IEEE Transactions on Pattern Analysis and Machine Intelligence*, vol. PP, no. 99, pp. 1–1, 2016.

[25] L. Tao, A. Paiement, D. Aldamen, M. Mirmehdi, S. Hannuna, M. Camplani, T. Burghardt, and I. Craddock, "A comparative study of pose representation and dynamics modelling for online motion quality assessment," *Computer Vision and Image Understanding*, November 2015.

[26] "Amazon Mechanical Turk." https://www.mturk.com/mturk/welcome. Accessed: 16-11-2013.

[27] A. Biess, D. G. Liebermann, and T. Flash, "A computational model for redundant human three-dimensional pointing movements: integration of independent spatial and temporal motor plans simplifies movement dynamics," *The Journal of Neuroscience*, vol. 27, no. 48, pp. 13045–13064, 2007.

[28] F. Arce, I. Novick, M. Shahar, Y. Link, C. Ghez, and E. Vaadia, "Differences in context and feedback result in different trajectories and adaptation strategies in reaching," *PLoS One*, vol. 4, no. 1, p. e4214, 2009.

[29] K. M. Mosier, R. A. Scheidt, S. Acosta, and F. A. Mussa-Ivaldi, "Remapping hand movements in a novel geometrical environment," *Journal of neurophysiology*, vol. 94, no. 6, pp. 4362–4372, 2005.

[30] Z. Danziger and F. A. Mussa-Ivaldi, "The influence of visual motion on motor learning," *The Journal of Neuroscience*, vol. 32, no. 29, pp. 9859–9869, 2012.

[31] A. S. Gordon, "Automated video assessment of human performance," in *Proceedings of AI-ED*, pp. 16–19, 1995.

[32] M. Jug, J. Perš, B. Dežman, and S. Kovačič, "Trajectory based assessment of coordinated human activity," *3rd International Conference on Computer Vision Systems (ICVS)*, vol. 2626, pp. 534–543, 2003.

[33] M. Perše, M. Kristan, J. Perš, and S. Kovačič, "Automatic evaluation of organized basketball activity using bayesian networks," *Computer Vision Winter Workshop (CVWW)*, pp. 11–18, 2007.

[34] J. K. Aggarwal and M. S. Ryoo, "Article 16 (43 pages)-human activity analysis: A review," *ACM Computing Surveys*, vol. 43, no. 3, 2011.

[35] N. Shroff, P. Turaga, and R. Chellappa, "Moving vistas: Exploiting motion for describing scenes," in *Computer Vision and Pattern Recognition (CVPR), 2010 IEEE Conference on*, pp. 1911–1918, IEEE, 2010.

[36] N. Stergiou and L. M. Decker, "Human movement variability, nonlinear dynamics, and pathology: is there a connection?," *Human Movement Science*, vol. 30, no. 5, pp. 869–888, 2011.

[37] S. Ali, A. Basharat, and M. Shah, "Chaotic invariants for human action recognition," in *IEEE International Conference on Computer Vision*, pp. 1–8, Oct. 2007.

[38] J. B. Dingwell and J. P. Cusumano, "Nonlinear time series analysis of normal and pathological human walking," *Chaos: An Interdisciplinary Journal of Nonlinear Science*, vol. 10, no. 4, pp. 848–863, 2000.

[39] J. B. Dingwell and H. G. Kang, "Differences between local and orbital dynamic stability during human walking," *Journal of Biomechanical Engineering*, vol. 129, no. 4, pp. 586–593, 2007.

[40] R. T. Harbourne and N. Stergiou, "Movement variability and the use of nonlinear tools: principles to guide physical therapist practice," *Physical Therapy*, vol. 89, no. 3, pp. 267–282, 2009.

[41] I. N. Junejo, E. Dexter, I. Laptev, and P. Pérez, "View-independent action recognition from temporal self-similarities," *IEEE Transactions on Pattern Analysis and Machine Intelligence*, vol. 33, no. 1, pp. 172–185, 2011.

[42] D. J. Miller, N. Stergiou, and M. J. Kurz, "An improved surrogate method for detecting the presence of chaos in gait," *Journal of biomechanics*, vol. 39, no. 15, pp. 2873–2876, 2006.

[43] M. Perc, "The dynamics of human gait," *European journal of physics*, vol. 26, no. 3, pp. 525–534, 2005.

[44] L. R. F. d'Alche Buc, "Dynamical modeling with kernels for nonlinear time series prediction," in *Advances in Neural Information Processing Systems 16: Proceedings of the 2003 Conference*, vol. 16, p. 129, MIT Press, 2004.

[45] A. Bissacco, A. Chiuso, Y. Ma, and S. Soatto, "Recognition of human gaits," in *IEEE Conference on Computer Vision and Pattern Recognition*, pp. 52–57, 2001.

[46] A. Bissacco, "Modeling and learning contact dynamics in human motion," in *IEEE Conference on Computer Vision and Pattern Recognition*, pp. 421–428, June 2005.

[47] H. D. Abarbanel, *Analysis of observed chaotic data*. New York: Springer-Verlag, 1996.

[48] G. P. Williams, *Chaos theory tamed*. Joseph Henry Press, 1997.

[49] F. Takens, *Detecting strange attractors in turbulence*. Springer, 1981.

[50] M. B. Kennel, R. Brown, and H. D. Abarbanel, "Determining embedding dimension for phase-space reconstruction using a geometrical construction," *Physical review A*, vol. 45, no. 6, p. 3403, 1992.

[51] M. Small, *Applied nonlinear time series analysis: applications in physics, physiology and finance*, vol. 52. World Scientific Publishing Company Incorporated, 2005.

[52] T. TenBroek, R. Van Emmerik, C. Hasson, and J. Hamill, "Lyapunov exponent estimation for human gait acceleration signals," *Journal of Biomechanics*, vol. 40, no. 2, p. 210, 2007.

[53] M. T. Rosenstein, J. J. Collins, and C. J. De Luca, "A practical method for calculating largest lyapunov exponents from small data sets," *Physica D: Nonlinear Phenomena*, vol. 65, no. 1, pp. 117–134, 1993.

[54] A. Wolf, J. B. Swift, H. L. Swinney, and J. A. Vastano, "Determining lyapunov exponents from a time series," *Physica D: Nonlinear Phenomena*, vol. 16, no. 3, pp. 285–317, 1985.

[55] R. Osada, T. Funkhouser, B. Chazelle, and D. Dobkin, "Shape distributions," *ACM Transactions on Graphics (TOG)*, vol. 21, no. 4, pp. 807–832, 2002.

[56] V. Venkataraman, P. Turaga, N. Lehrer, M. Baran, T. Rikakis, and S. L. Wolf, "Attractor-shape for dynamical analysis of human movement: Applications in stroke rehabilitation and action recognition," in *IEEE Conference on Computer Vision and Pattern Recognition Workshops (CVPRW)*, pp. 514–520, IEEE, 2013.

[57] N. Krishnamurthi, S. Mulligan, P. Mahant, J. Samanta, and J. J. Abbas, "Deep brain stimulation amplitude alters posture shift velocity in parkinson's disease," *Cognitive Neurodynamics*, vol. 6, no. 4, pp. 325–332, 2012.

[58] M. L. Pickerill and R. A. Harter, "Validity and reliability of limits-of-stability testing: a comparison of 2 postural stability evaluation devices," *Journal of Athletic Training*, vol. 46, no. 6, pp. 600–606, 2011.

[59] H. Abarbanel, *Analysis of Observed Chaotic data*. Springer Science & Business Media, 2012.

[60] V. Venkataraman and P. Turaga, "Shape distributions of nonlinear dynamical systems for video-based inference," *arXiv preprint arXiv:1601.07471*, 2016.

[61] C.-C. Chang and C.-J. Lin, "LIBSVM: A library for support vector machines," *ACM Transactions on Intelligent Systems and Technology*, vol. 2, pp. 27:1–27:27, 2011. Software available at http://www.csie.ntu.edu.tw/~cjlin/libsvm.

[62] P.-T. Cheng, S.-H. Wu, M.-Y. Liaw, A. M. Wong, and F.-T. Tang, "Symmetrical body-weight distribution training in stroke patients and its effect on fall prevention," *Archives of physical medicine and rehabilitation*, vol. 82, no. 12, pp. 1650–1654, 2001.

[63] A. M. Wong, L. Ming-Yih, K. Jung-Kun, and T. Fuk-Tan, "The development and clinical evaluation of a standing biofeedback trainer," *Journal of rehabilitation research and development*, vol. 34, no. 3, p. 322, 1997.

[64] M. Müller, "Dynamic time warping," in *Information retrieval for music and motion*, ch. 4, pp. 69–84, Springer, 2007.

[65] Q. Wang, P. Turaga, G. Coleman, and T. Ingalls, "Somatech: an exploratory interface for altering movement habits," in *CHI'14 Extended Abstracts on Human Factors in Computing Systems*, pp. 1765–1770, ACM, 2014.

[66] P. Mazzoni, A. Hristova, and J. W. Krakauer, "Why don't we move faster? parkinson's disease, movement vigor, and implicit motivation," *The Journal of Neuroscience*, no. 27, pp. 7105–7116, 2007.

[67] J. Su, S. Kurtek, E. Klassen, and A. Srivastava, "Statistical analysis of trajectories on Riemannian manifolds: Bird migration, hurricane tracking, and video surveillance," *Annals of Applied Statistics*, vol. 8, no. 1, 2014.